

Towards a unified understanding of polymer cononsolvency: insights from the Flory-Huggins-Potts framework

Satyen Dhamankar and Michael A. Webb*

*Department of Chemical and Biological Engineering, Princeton University, Princeton, NJ
08544, USA*

E-mail: mawebb@princeton.edu

Abstract

In polymer solutions, the phenomenon of cononsolvency describes when mixing two good solvents creates poor-solvent conditions for the polymer over some specific composition range. Observations of cononsolvency typically relate to either phase separation at the macroscopic level or chain collapse at the microscopic level. Despite its technological and biophysical relevance, the connection between the macroscopic and microscopic observations of cononsolvency and how these differ by mechanism remains unclear. In this work, we distinguish between different mechanisms of cononsolvency using various models and observations derived from a single theoretical framework for polymer solutions. We first use mean-field analysis to identify energetic regimes, which are defined by sets of effective χ parameters, where changes in solvent/cosolvent composition induce phase separation. Next, to make a connection to the microscopic physics, we conduct Monte Carlo simulations of models with interactions that align with these effective χ parameters from these different regimes and observe correspond-

ing composition-induced coil-globule transitions. These transitions are elucidated with signatures associated with specific mechanisms of cononsolvency from the literature. Interestingly, systems with identical effective χ parameters can display different mechanisms at the microscopic level. Ultimately, these results provide new insights into cononsolvency that may help to distinguish amongst mechanisms or inform strategies to control polymer solution behavior.

1 Introduction

Cononsolvency in polymer solutions arises when mixing two individually good solvents yields poor-solvent conditions for a polymer. Under such conditions, at a macroscopic level, the solution may phase separate¹⁻⁵ or, at a microscopic level, the characteristic size of polymer chains may decrease.⁶⁻¹⁷ This composition-sensitive behavior has relevance across scientific and technological applications, such as detecting volatile organic compounds by measuring the response of a hydrogel,¹⁸ measuring enantiomeric excess in organic synthesis by observing the fluorescent enhancement,¹⁹ altering rates of organic reactions at liquid-liquid interfaces,²⁰ tuning the frictional properties of polymer brushes by adjusting solution composition,^{21,22} and affecting the transport of molecules through a porous polymer matrix.^{21,23,24} Furthermore, the physics governing cononsolvency has profound implications for understanding biological phase separation, protein denaturation,²⁵⁻³⁰ and cell recovery in tissues.³¹⁻³³ There is thus significant interest to understand polymer cononsolvency and related phenomena.

Multiple mechanisms of polymer cononsolvency have been reported on the basis of various theoretical and computational analyses. The preferential polymer-cosolvent adsorption mechanism suggests that the cosolvent, on trace addition, selectively solvates the polymer or facilitates formation of “enthalpic bridges” between otherwise distal parts of a polymer chain.³⁴ These interactions can then trigger phase separation or single-chain collapse.^{14,35-42} Effects akin to preferential adsorption can also be realized based purely on entropic fac-

tors, such as size asymmetry between solvent and cosolvent leading to effective depletion interactions.⁴³ In another scenario, the cosolvent is envisioned to act like a surfactant, such that polymer contraction allows the cosolvent to interact favorably with both solvent and polymer.⁴⁴ Another manifestation arises when solvent-cosolvent interactions are substantially more favorable than interactions with the polymer, such that the polymer sacrifices its entropy to encourage solvent-cosolvent mixing.^{4,13,16,43,45,46} The concept of geometric frustration has also been used to explain cononsolvency, proposing that competition between cosolvent and solvent with polymer destabilizes the polymer solvation environment.^{47,48} Overall, this literature highlights polymer cononsolvency as a complex phenomenon with various enthalpic and entropic factors informing distinct mechanistic views.

Elucidation of polymer cononsolvency has been approached with numerous theoretical and computational techniques. Previous studies using Flory-Huggins theory have demonstrated that phase separation can be induced when either solvent-cosolvent or polymer-solvent interactions dominate, even when the polymer is miscible with each solvent individually.^{45,49,50} Furthermore, analyses of structure factors obtained following application of the random phase approximation provide similar conclusions.⁵¹ Nevertheless, mean-field insights into the energetic factors driving phase separation do not directly translate into understanding microscopic physics, such as single-chain conformational behavior.³⁴ In this direction, field theoretic methods^{14,42} have demonstrated that single-chain collapse indeed occurs given strong, preferential affinity of the polymer for one of the solvents, but there is no apparent coil-globule transition driven purely by solvent-cosolvent affinity.

Molecular dynamics (MD) simulations of systems with generic chemical attributes (e.g., bead-spring polymers in monomeric solvents) have effectively illustrated many of the aforementioned mechanisms of cononsolvency at a microscopic level.^{34,43,52} A typical observation from such simulations is that the radius of gyration for a single polymer chain first decreases and then increases as cosolvent is progressively added. This scenario has been induced by

solvent-cosolvent mixing, preferential polymer-solvent adsorption, and the surfactant-like action of the cosolvent by analyzing the molecular environment of the polymer and carefully evaluating molecular affinities.^{34,48,53-55} In chemically specific systems, such as poly(N-isopropylacrylamide) in water and ethanol, single-chain collapse, consistent with cononsolvency, has been observed, but there is debate as to what precise interactions beget this behavior.⁵⁶⁻⁵⁹ While various forms of cononsolvency have been observed, mechanisms are typically studied using different models and approaches, with macroscopic (solution-phase) and microscopic (single-chain) behaviors rarely considered together.

Here, we investigate the phenomenological origins of cononsolvency and the connection between its macroscopic and microscopic manifestations using a single theoretical framework. In particular, we adapt the recently developed Flory-Huggins-Potts framework, which extends traditional Flory-Huggins theory by incorporating orientation-dependent interactions. This approach was effective for capturing complex thermoresponsive behaviors in polymer solutions, including heating-induced phase separation and coil-globule transitions.⁶⁰ Leveraging this framework, we explore how varying interaction strengths and types influence system response to solvent-cosolvent composition shifts and how these responses align with proposed cononsolvency mechanisms. We first analyze phase behavior at the mean-field level, identifying energetic regimes that yield phase separation through stability analysis of ternary solutions. Using simulation parameters derived from these regimes, we then examine single-chain conformations in solvent-cosolvent mixtures via Monte Carlo simulations. Our results show strong correspondence between macroscopic phase behavior and single-chain conformational characteristics. Further analysis enables identification of distinct cononsolvency mechanisms based on the underlying energetic regime, defined by mean-field theory alone, and the specific type of interactions, which require a microscopic description of the system. Together, this work provides new insights into cononsolvency manifestations and offers a framework for distinguishing mechanisms based on macroscopic and microscopic observations.

2 Methods

2.1 Flory-Huggins-Potts framework

We extend the recently developed Flory-Huggins-Potts (FHP) framework⁶⁰ to model ternary polymer solutions. In effect, the FHP framework extends conventional Flory-Huggins theory by assigning internal states to particles that modulate pairwise interactions. These states may be interpreted, for example, as capturing aspects of molecular orientation at a coarse-grained resolution, enabling expression of orientation-dependent interactions, whereas traditional FH assumes isotropic interactions. In previous work, we showed that orientation-dependent interactions, particularly between monomer and solvent, can produce closed-loop and hourglass-shaped binodals and heating-induced coil-globule transitions. In FH theory, these phenomena are captured by using temperature-dependent interaction parameters. This led us to hypothesize that anisotropic interactions may also be crucial in cononsolvency, a hypothesis that we explore subsequently. While the motivation and detailed development of the FHP framework can be found in Ref. 60, we briefly review some salient aspects.

The behavior of the FHP model is governed by a well-defined Hamiltonian. We consider a fully occupied lattice of polymer, solvent, and cosolvent sites, with the system energy given by bonded and non-bonded contributions:

$$\mathcal{H} = \frac{1}{2} \sum_{i=1}^n \sum_{j \in \mathcal{N}(i)} \epsilon(\alpha_i, \alpha_j, \hat{\sigma}_i, \hat{\sigma}_j) + \sum_{k=1}^{N_p} \sum_{l=1}^{N_m-1} V(\vec{r}_{l+1}^{(k)}, \vec{r}_l^{(k)}), \quad (1)$$

where α_i is the species type (monomer ‘m’, solvent ‘s’, or cosolvent ‘c’) and $\hat{\sigma}_i$ is the unit vector representing the orientation of the particle at site i , and $\mathcal{N}(i)$ is the set of particles with which i interacts. The function $\epsilon(\cdot)$ defines pairwise interaction energies, n is the total number of lattice sites, N_p is the number of polymer chains, N_m is the number of monomers per chain, and $\vec{r}_l^{(k)}$ is the position of the l th monomer in chain k . The potential $V(\cdot)$ ensures

bonded monomers remain within $\mathcal{N}(i)$. The non-bonded interaction term is defined as:

$$\epsilon(\alpha_i, \alpha_j, \hat{\sigma}_i, \hat{\sigma}_j) = \epsilon_{\alpha_i \alpha_j}^{\parallel} + \Lambda(i, j) \Delta_{\alpha_i \alpha_j}, \quad (2)$$

where $\Delta_{\alpha_i \alpha_j} = \epsilon_{\alpha_i \alpha_j}^{\parallel} - \epsilon_{\alpha_i \alpha_j}^{\#}$ captures the difference between aligned and misaligned interactions, and $\Lambda(i, j) \in [0, 1]$ distinguishes the degree of alignment. For convenience, we assume aligned interactions are stronger, so $\Delta_{\alpha_i \alpha_j} \leq 0$. When $\Lambda(i, j)$ or $\Delta_{\alpha_i \alpha_j} = 0$, interactions are isotropic, and FHP reduces to standard Flory-Huggins theory.

We investigate $\Lambda(i, j)$ with a form given by

$$\Lambda_{\text{corr}}(i, j) = \Theta(\hat{\sigma}_i \cdot \hat{\sigma}_j - \delta) \quad (3)$$

where $\Theta(\cdot)$ is the Heaviside step function, and δ defines the angular tolerance for alignment. We refer to this interaction style as a ‘‘correlation network,’’ and it resembles interactions in Maier-Saupe theory.⁶¹ Correlation networks allow all neighbors to align cooperatively, since the function becomes nonzero when two vectors point nominally in the same direction. This is perhaps reminiscent to the collective ordering observed in nematic liquid crystals or hydrogen-bonding networks in water, where molecular orientations enable multiple simultaneous interactions.

2.2 Helmholtz energy by mean-field analysis

Macroscopic phase behavior in the FHP framework is evaluated in the context of mean-field theory. All systems are considered incompressible, such that the total volume is given by $V = \sum_i n_i v_i$ where n_i is the mole number and v_i the molar volume of species i . If each polymer segment occupies one lattice site of volume v_0 , then $v_p = N_m v_0$. The system composition is described by volume fractions $\phi_i = (n_i v_i)/V$, with $\sum_{i \in \{p, s, c\}} \phi_i = 1$.

Following Ref. 60, but extended to three components, the intensive free energy of mixing

per lattice site is:

$$\beta\Delta f_{\text{mix}} = \sum_i \frac{\phi_i}{(v_i/v_0)} \ln \phi_i + \frac{1}{2} \sum_j \sum_{k \neq j} \phi_j \phi_k \chi_{jk}^{\text{FHP}}, \quad (4)$$

where $\beta = (k_{\text{B}}T)^{-1}$ and χ_{ij}^{FHP} are FHP interaction parameters (with $\chi_{ii}^{\text{FHP}} = 0$). This expression mirrors the ternary Flory-Huggins form but with modified interaction terms:

$$\chi_{ij}^{\text{FHP}}(T) = \beta(z-2) \left(\epsilon_{ij}^{\parallel} - \frac{1}{2}(\epsilon_{ii}^{\parallel} + \epsilon_{jj}^{\parallel}) \right) + \tilde{\chi}_{ij}(T), \quad (5)$$

where the first term is essentially the Flory-Huggins χ at the misaligned energy scale, z is the coordination number on the lattice, and $\tilde{\chi}_{ij}(T)$ is a perturbation term that accounts for the difference between aligned and misaligned interactions. In particular,

$$\tilde{\chi}_{ij}(T) = \beta(z-2)p_v \left(\tilde{\Delta}_{ij}(T) - \frac{1}{2}(\tilde{\Delta}_{ii}(T) + \tilde{\Delta}_{jj}(T)) \right) \quad (6)$$

where $\tilde{\Delta}_{ij}(T)$ accounts for the free energy difference between aligned and misaligned states:

$$\tilde{\Delta}_{ij}(T) = \frac{\Delta_{ij}}{1 + \left(\frac{1-p_{\Omega}}{p_{\Omega}} \right) \exp(\Delta_{ij}/k_{\text{B}}T)}. \quad (7)$$

The terms p_v and p_{Ω} are geometric factors related to what defines aligned interactions. In particular, p_v is the fraction of neighbors that can form aligned interactions, and p_{Ω} is the fraction of pairwise orientations that are classified as aligned for such neighbors.

For simplicity, all numerical results correspond to a simple cubic lattice where $\mathcal{N}(i)$ includes the nearest, next-nearest, and next-next-nearest neighbors of site i , yielding $z = 26$. Furthermore, polymers are monodisperse with $N_{\text{m}} = 32$, such that the volume occupied by a polymer chain is $v_{\text{p}} = 32v_0$. The volume occupied by each solvent particle and cosolvent particle is v_0 . For the purpose of computing p_v and p_{Ω} , particle orientations are restricted to direct towards one of 26 neighboring sites. All energetic parameters are associated with

a fundamental energy scale of ϵ_0 .

2.3 Characterization of phase behavior

The phase behavior of the system can be determined from Eq. (4) by specifying the composition $\boldsymbol{\phi} = (\phi_p, \phi_s, \phi_c)$, the molar volumes $\boldsymbol{v} = (v_p, v_s, v_c)$, and the interaction parameters $\mathbf{X}^{\text{FHP}} = (\chi_{\text{ps}}^{\text{FHP}}, \chi_{\text{pc}}^{\text{FHP}}, \chi_{\text{sc}}^{\text{FHP}})$. Briefly, the stability of a homogeneous mixture is assessed by examining the sign of the determinant of the Hessian for the Helmholtz energy:

$$|\mathbf{H}| = \frac{\partial^2 \beta \Delta f_{\text{mix}}}{\partial \phi_A^2} \cdot \frac{\partial^2 \beta \Delta f_{\text{mix}}}{\partial \phi_B^2} - \left(\frac{\partial^2 \beta \Delta f_{\text{mix}}}{\partial \phi_A \partial \phi_B} \right)^2. \quad (8)$$

The spinodal boundary is defined by the locus of points for which $|\mathbf{H}| = 0$, while negative values indicate an unstable mixture that would undergo phase separation. Here, we use the condition $|\mathbf{H}| < 0$ over some composition range as the criterion for determining whether a system exhibits cononsolvency at a macroscopic level.

For select systems that meet the criterion above, their phase behavior is more precisely characterized by mapping binodal boundaries and determining the compositions of coexisting phases. Binodal boundaries are computed by first identifying critical points using constraints involving third-order derivatives:^{62,63}

$$\frac{\partial |\mathbf{H}|}{\partial \phi_A} \cdot \frac{\partial^2 \beta \Delta f_{\text{mix}}}{\partial \phi_B^2} - \frac{\partial |\mathbf{H}|}{\partial \phi_B} \cdot \frac{\partial^2 \beta \Delta f_{\text{mix}}}{\partial \phi_A \partial \phi_B} = 0 \quad (9)$$

and

$$\frac{\partial |\mathbf{H}|}{\partial \phi_B} \cdot \frac{\partial^2 \beta \Delta f_{\text{mix}}}{\partial \phi_A^2} - \frac{\partial |\mathbf{H}|}{\partial \phi_A} \cdot \frac{\partial^2 \beta \Delta f_{\text{mix}}}{\partial \phi_A \partial \phi_B} = 0. \quad (10)$$

Following identification of a critical point, coexistence lines are extended using a recently proposed natural parameter continuation algorithm⁶⁴ akin to Gibbs-Duhem integration. As this approach iteratively identifies different compositions with equivalent chemical potentials, it also facilitates the construction of tie lines to indicate the equilibrium compositions of the

coexisting phases. For additional details regarding this algorithm or the utilization of eqs. (8)-(10), readers are referred to Ref. 64 and the references therein.

2.4 Monte Carlo simulations

To characterize cononsolvency at a microscopic level, we perform lattice Monte Carlo (MC) simulations. The MC simulations directly implement specific manifestations of the Hamiltonian defined by eq. (1). These simulations are performed only for systems with parameters that exhibit mixture instability (Table 1). All simulations feature a $34 \times 34 \times 34$ simple cubic lattice with periodic boundaries and unit edge length; lattice sites are occupied by a mixture of solvent and cosolvent particles and a single polymer chain ($N_m = 32$). For each manifestation of a Hamiltonian, simulations are performed over a set of cosolvent fractions that approximately (within the limits afforded by the discrete lattice) correspond to $x_c \in [0, 1]$ in increments of 0.1. Additionally, sampling is conducted at temperatures given by $\beta^{-1} = k_B T = 0.9\epsilon_0, 1.0\epsilon_0,$ and $1.1\epsilon_0$ (see Supplemental Information, Figure S1).

Systems are initialized by placing polymer chains on lattice sites using a self-avoiding random walk. Cosolvent particles are then randomly distributed across the remaining sites to achieve the target mole fraction, and any unoccupied sites are filled with solvent particles. All particles are randomly assigned one of 26 possible orientations with uniform probability. Configurational sampling is performed using a variety of MC moves. For solvent and cosolvent particles, these include orientation exchanges, collective orientation perturbations, and particle swaps. Polymer moves include end-rotation, forward and backward reptation, and chain regrowth with orientation updates. Orientation updates are also applied to solvent particles in contact with the polymer and to a randomly selected subset of lattice particles. See Table S1 in the Supporting Information for a summary of all moves. All move types are attempted with equal probability. Each simulation consists of 10^8 MC moves, with configurations sampled every 10^4 moves. The first half of each simulation is used for equilibration and the second half for collecting production data (see Supporting Information, Fig. S2).

For each condition (parameter set, composition, and temperature), thirty independent simulations are performed for statistical analysis and uncertainty quantification. In addition, to compute certain properties for an ideal mixture, thirty independent simulations are also run under athermal conditions (i.e., all energy parameters except the bonding and implied excluded-volume interactions are set to zero).

2.5 Conformational analysis

Polymer size is characterized by the radius of gyration R_g . For a polymer with N_m monomers at positions \mathbf{r}_i , the radius of gyration is computed using

$$R_g = \sqrt{\frac{1}{N_m} \sum_{i=1}^{N_m} (\mathbf{r}_i - \mathbf{r}_{\text{com}})^2}, \quad (11)$$

with the polymer center of mass defined per usual

$$\mathbf{r}_{\text{com}} = \frac{1}{N_m} \sum_{i=1}^{N_m} \mathbf{r}_i. \quad (12)$$

For consistent comparisons across conditions, we report a normalized radius of gyration, $\frac{\langle R_g \rangle}{\langle R_g \rangle_{\text{ath}}}$, where $\langle R_g \rangle$ is the ensemble-averaged R_g for a given system and $\langle R_g \rangle_{\text{ath}}$ is a reference given by an athermal simulation incorporating only excluded-volume interactions. For chains with $N_m = 32$, we empirically find that $\langle R_g \rangle_{\text{ath}} = 3.83 \pm 0.003$. For simplicity, we use $\langle R_g \rangle_{\text{ath}} = 3.83$ in our calculations.

2.6 Solvation analysis

To distinguish cononsolvency mechanisms at the single-chain level, we compare the local solvation environment of the polymer from Monte Carlo simulations with ideal-mixing pre-

dictions. Deviations are quantified by the normalized excess number of interactions

$$\begin{aligned} N_{\kappa}^{\text{ex}} &= N_{\kappa} - N_{\kappa}^{\text{id}} \\ \frac{N_{\kappa}^{\text{ex}}}{N_{\kappa}^{\text{id}}} &= \frac{N_{\kappa}}{N_{\kappa}^{\text{id}}} - 1 = \tilde{N}_{\kappa} - 1 \end{aligned} \quad (13)$$

where N_{κ} specifies the number of interactions under some restriction κ , and the superscripts ‘ex’ and ‘id’ indicate excess and ideal values, respectively. The restriction of κ for our analysis relates to some pairing of specific species or particles and/or whether interactions are aligned versus misaligned.

The number of pairwise interactions between monomer, solvent, and cosolvent particles is computed as

$$N_{\text{mm}} = \frac{1}{2} \sum_{i \in \mathcal{P}} \sum_{j \in \mathcal{N}(i)} \mathbf{1}_j^{\mathcal{P}}, \quad (14)$$

$$N_{\text{ms}} = \sum_{i \in \mathcal{P}} \sum_{j \in \mathcal{N}(i)} \mathbf{1}_j^{\mathcal{S}}, \quad (15)$$

$$N_{\text{mc}} = \sum_{i \in \mathcal{P}} \sum_{j \in \mathcal{N}(i)} \mathbf{1}_j^{\mathcal{C}}, \quad (16)$$

$$N_{\text{sc}} = \sum_{i \in \mathcal{S}} \sum_{j \in \mathcal{N}(i)} \mathbf{1}_j^{\mathcal{C}}. \quad (17)$$

where $N_{\alpha_i \alpha_j}$ indicates the number of unique interactions between species α_i and α_j and \mathcal{P} , \mathcal{S} , and \mathcal{C} respectively denote the sets of all polymer, solvent, and cosolvent particles, and $\mathbf{1}_j^{\mathcal{X}}$ is an indicator function equal to unity if the indexed particle j is in the set \mathcal{X} and zero otherwise.

To count only interactions directly involved with solvation, we define the solvation shell of the polymer as the union of all non-polymer particles in its neighborhood:

$$\mathcal{P}_{\text{sc}} = \bigcup_{i \in \mathcal{P}} (\mathcal{N}(i) \setminus \mathcal{P}) = \mathcal{P}_{\text{s}} \cup \mathcal{P}_{\text{c}}, \quad (18)$$

where \mathcal{P}_s and \mathcal{P}_c now denote sets of solvent and cosolvent particles within \mathcal{P}_{sc} , which is the set of all solvent and cosolvent particles within the neighborhood of \mathcal{P} . The number of aligned solvent-cosolvent interactions within the solvation shell follows as

$$N_{sc|\mathcal{P}_{sc}}^{\parallel} = \sum_{i \in \mathcal{P}_s} \sum_{j \in \mathcal{N}(i)} \mathbf{1}_j^c \cdot \Lambda(i, j) + \sum_{i \in \mathcal{P}_c} \sum_{\substack{j \in \mathcal{N}(i) \\ j \notin \mathcal{P}_s}} \mathbf{1}_j^c \cdot \Lambda(i, j), \quad (19)$$

where $\Lambda(i, j)$ is alignment function defined for the interaction type.

For ideal references, we first empirically determine N_{mm}^{id} from MC simulation of an athermal chain. Subsequently, the quantities N_{ms}^{id} and N_{mc}^{id} are inferred via

$$N_{ms}^{\text{id}} = (1 - x_c) N_{ms \cup mc}^{\text{id}}, \quad (20)$$

$$N_{mc}^{\text{id}} = x_c N_{ms \cup mc}^{\text{id}}, \quad (21)$$

and

$$N_{ms \cup mc}^{\text{id}} = z N_m - 2 N_{mm}^{\text{id}}, \quad (22)$$

where the last expression for the number of either monomer-solvent or monomer-cosolvent interactions exploits the restriction that the overall number of interactions involving the polymer is conserved on the lattice. For chains with $N_m = 32$, we estimate N_{mm}^{id} by computing the average number of monomer-monomer interactions from athermal simulations of a chain in solvent. These simulations yield $\langle N_{mm} \rangle_{\text{ath}} = 62.91 \pm 0.04$. We note that a chain with N_m monomers must have at least $N_m - 1$ interactions, accounting for bonded neighbors, making the result above approximately and empirically $2N_m - 1$. For simplicity, we use $N_{mm}^{\text{id}} = 63$ in all calculations. Similarly, the expected number of solvent-cosolvent interactions is approximated as

$$N_{sc}^{\text{id}} = z N_s x_c. \quad (23)$$

We further probe polymer solvation by defining a relative solvation score

$$\text{RSS} = \frac{|\mathcal{P}_\kappa|}{zN_m}, \tag{24}$$

where $|\mathcal{X}|$ denotes the cardinality (i.e., number of elements) of the set \mathcal{X} , which here corresponds to some condition κ on \mathcal{P} . For analysis, we consider both the total number of solvent/cosolvent particles in the solvation shell, $|\mathcal{P}_{\text{sc}}|$, as well as the individual contributions by solvent, $|\mathcal{P}_s|$, and cosolvent, $|\mathcal{P}_c|$. The normalizing factor zN_m represents the number of solvent/cosolvent particles in neighborhood of a monomer, if every monomer were isolated in solvent. In a polymer, the maximum number of solvent particles within \mathcal{P}_{sc} would be $z(N_m - 2) + 2$, which approaches zN_m for large N_m . Thus, Eq. (24) measures the average solvent/cosolvent exposure per monomer, analogous to the normalized number of water molecules in the first solvation shell (NFSS) used to assess hydration frustration in proteins.⁶⁵

To assess the relative strength of cohesion versus solvation in the system, we introduce a relative cohesion–solvation ratio (RCSR):

$$\text{RCSR} = \frac{\tilde{N}_{\text{mm}} + \tilde{N}_{\text{sc}}}{\tilde{N}_{\text{ms}} + \tilde{N}_{\text{mc}}}. \tag{25}$$

This dimensionless quantity thereby provides a scalar measure that contrasts cohesive interactions against solvation-driven interactions in the system.

3 Results

3.1 Analysis of phase behavior

We first use mean-field theory to identify parameter regimes exhibiting phase behavior consistent with cononsolvency. Under the constraint that all components are mutually misci-

ble ($\chi_{ij}^{\text{FHP}} < 0 \forall i, j$), we systematically explore the interaction-parameter space $\mathbf{X}^{\text{FHP}} = (\chi_{\text{ps}}^{\text{FHP}}, \chi_{\text{pc}}^{\text{FHP}}, \chi_{\text{sc}}^{\text{FHP}})$ and identify parameter sets for which $|\mathbf{H}| < 0$, signaling instability and thus phase separation (Fig. 1a). This analysis reveals distinct parameter regions characterized by the strongest interaction type present. We denote by \mathcal{R}_{ij} the region of parameter space where ($\chi_{ij}^{\text{FHP}} < \chi_{ik}^{\text{FHP}}, \chi_{jk}^{\text{FHP}} \leq 0$), implying that the strongest attractive interaction is between species i and j . Thus, three non-overlapping parameter regimes emerge— \mathcal{R}_{sc} , \mathcal{R}_{ps} , and \mathcal{R}_{pc} —each potentially displaying cononsolvency based on macroscopic criteria.

The emergence of cononsolvency, in terms of competing interactions, can be understood by examining successive cross sections in Fig. 1a. Initially, at $\chi_{\text{sc}}^{\text{FHP}} = 0$, two distinct regions, \mathcal{R}_{ps} and \mathcal{R}_{pc} , exhibit phase separation for a broad range of parameters, for which polymer-solvent or polymer-cosolvent interactions are strongly favorable relative to interactions between solvent and cosolvent (Fig. 1b). As solvent-cosolvent interactions become increasingly favorable (more negative $\chi_{\text{sc}}^{\text{FHP}}$), the areas of \mathcal{R}_{ps} and \mathcal{R}_{pc} shrink, as interactions are more balanced. Concurrently, a third region, \mathcal{R}_{sc} , emerges where solvent-cosolvent interactions dominate (Fig. 1c). Eventually, as solvent-cosolvent affinity strengthens further, \mathcal{R}_{ps} and \mathcal{R}_{pc} vanish entirely, leaving an expanded \mathcal{R}_{sc} region (Fig. 1d,e). This analysis provides a baseline expectation, consistent with prior work,⁵⁰ that cononsolvency can be driven by different dominant interaction types—whether polymer-solvent, polymer-cosolvent, or solvent-cosolvent.

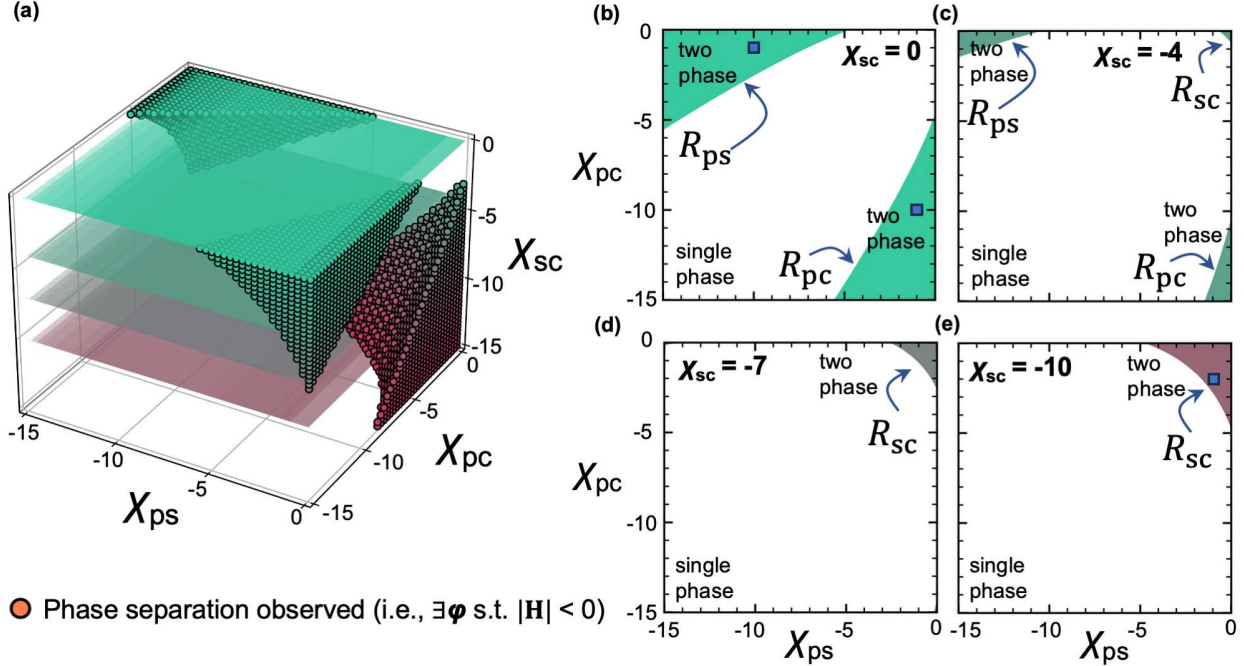


Figure 1: Classification of phase behavior for ternary polymer solutions described by the Flory-Huggins-Potts (FHP) framework. (a) Regions in interaction parameter space $\mathbf{X}^{\text{FHP}} = (\chi_{\text{ps}}^{\text{FHP}}, \chi_{\text{pc}}^{\text{FHP}}, \chi_{\text{sc}}^{\text{FHP}})$ where phase separation is required at some composition ϕ , as determined by the mean-field stability criterion ($|\mathbf{H}| < 0$). Markers indicate parameter sets that yield instability; cross-sectional planes at $\chi_{\text{sc}}^{\text{FHP}} = 0, -4, -7$, and -10 correspond to panels (b–e). (b–e) Two-dimensional slices of (a) showing phase behavior as a function of $\chi_{\text{ps}}^{\text{FHP}}$ and $\chi_{\text{pc}}^{\text{FHP}}$ for fixed values of $\chi_{\text{sc}}^{\text{FHP}}$. Shaded regions indicate parameter combinations that guarantee phase separation at some composition. Regions of observed two-phase coexistence are labeled \mathcal{R}_{sc} , \mathcal{R}_{ps} , and \mathcal{R}_{pc} , according to the most negative interaction parameter. Square markers denote parameter sets selected for further analysis in Fig. 2.

Prior work has suggested that the shape, location, and extent of coexistence regions, as well as the orientation of tie lines, may reflect distinct underlying mechanisms of cononsolvency.⁵⁰ To investigate this, we constructed full ternary phase diagrams for representative parameter sets drawn from each of the three regimes: \mathcal{R}_{ps} , \mathcal{R}_{pc} , and \mathcal{R}_{sc} (see blue squares in Fig. 1b,e). While all selected systems are guaranteed to exhibit phase separation at certain compositions, the resulting phase diagrams indeed differ in the shapes of their binodal curves and the orientations of their tie lines based on the dominant interaction present in the system (Fig. 2a–c). In the case where polymer-solvent interactions dominate (Fig. 2a), the tie lines predominantly connect phases in which one is rich in polymer and solvent, while the other is

rich in cosolvent and depleted in polymer. Due to the arbitrary labeling of solvent and cosolvent, which have equivalent molecular volumes, Fig. 2a and Fig. 2b are related by exchange symmetry. Accordingly, when polymer-cosolvent interactions prevail (Fig. 2b)—the tie lines connect a polymer/cosolvent-rich phase with a polymer-lean, solvent-rich phase. In contrast, when solvent-cosolvent interactions dominate (Fig. 2c), the tie lines orient nearly perpendicular to the polymer composition axis, leading to coexistence between a very polymer-lean phase with mixed solvent and a polymer-rich phase. Together, these observations highlight that, within the same theoretical framework, cononsolvency can emerge in multiple ways with distinct signatures in terms of the orientation and symmetry of tie lines. Ultimately, while these observations may serve as useful indicators of the dominant underlying interactions, they remain qualitative and do not offer insight into the microscopic details of how cononsolvency manifests.

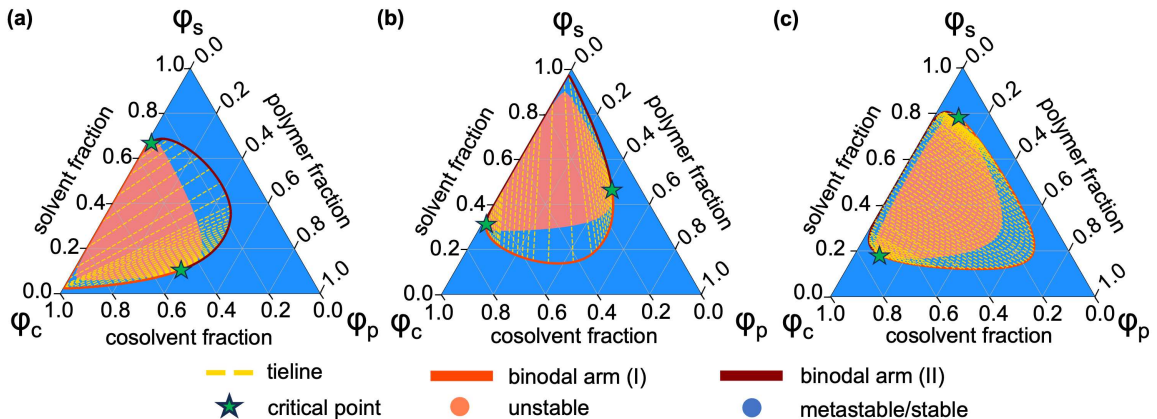


Figure 2: Ternary phase diagrams for representative systems that exhibit phase separation in the Flory-Huggins-Potts (FHP) framework. The specific parameter sets $\mathbf{X}^{\text{FHP}} = (\chi_{\text{ps}}^{\text{FHP}}, \chi_{\text{pc}}^{\text{FHP}}, \chi_{\text{sc}}^{\text{FHP}})$ are drawn from the regions (a) \mathcal{R}_{ps} with $\mathbf{X}^{\text{FHP}} = (-10, -1, 0)$, (b) \mathcal{R}_{pc} with $\mathbf{X}^{\text{FHP}} = (-1, -10, 0)$, and (c) \mathcal{R}_{sc} with $\mathbf{X}^{\text{FHP}} = (-1, -2, -10)$. The positions of these parameter sets are shown as blue squares in Fig. 1. A representative set of tie lines (yellow, dashed lines) are shown. The tie lines connect points of specific compositions on two distinct binodal arms (I and II) where the chemical potentials of the constituent species are equal, resulting in equilibrium phase coexistence. The green stars indicate critical points. The peach coloring highlights regions of instability for a homogeneous mixture (i.e., spinodal regions).

3.2 Analysis of single-chain behavior

The preceding results demonstrate how specific combinations of mean-field interaction parameters can induce macroscopic phase separation across a range of ternary compositions. We now turn to the question of whether such macroscopic behavior is echoed in distinct microscopic manifestations of cononsolvency, such as a coil-globule transition induced by solvent-mixture composition. To address this, we perform Monte Carlo (MC) simulations to study the conformation and solvation of a single polymer chain in mixed solvents for three systems (Table 1) with Hamiltonians representative of the phase behavior shown in Fig. 2b,c. In the following sections, we provide a brief summary of the systems and key results and then subsequently examine each in more detail.

Table 1: Parameters used in Monte Carlo simulations of Flory-Huggins-Potts models.

Label	χ_{ps}^{FHP}	χ_{pc}^{FHP}	χ_{sc}^{FHP}	$\epsilon_{mm}^{\#}$	$\epsilon_{ms}^{\#}$	$\epsilon_{mc}^{\#}$	$\epsilon_{sc}^{\#}$	Δ_{mm}	Δ_{ms}	Δ_{mc}	Δ_{sc}	p_v^{ms}	p_v^{sc}
\mathcal{R}_{pc}°	-1	-10	0	-1	-0.541	-0.583	-0.416	0	0	0	0	0	0
\mathcal{R}_{sc}°	-1	-2	-10	-1	-0.541	-0.916	0	0	0	0	0	0	0
$\mathcal{R}_{sc}^{\wedge}$	-1	-2	-10	-1	-0.4	-0.583	0	0	-0.421	0	-0.917	1.0	1.0

3.2.1 Overview of systems and mechanisms

All systems exhibit a reduction in the radius of gyration for the polymer chain, R_g , in mixed solvents compared to pure solvent or cosolvent (Fig. 3), which is a commonly referenced signature of cononsolvency. Based on further analysis of the solvation environment around the polymer, we then associate these chain collapses with specific mechanisms described in the literature. One system, labeled \mathcal{R}_{pc}° , uses a parameter set from \mathcal{R}_{pc} (Fig. 2b) and incorporates only isotropic interactions (i.e., $\Delta_{ij} = 0 \forall i, j$). We associate chain collapse in this regime with a so-called preferential adsorption (PA) mechanism. The collapse occurs when the cosolvent to solvent ratio is relatively low (Fig. 3a). The other two systems use distinct microscopic parameter sets that yield the same \mathbf{X}^{FHP} value within \mathcal{R}_{sc} . The key distinction between the two systems is that one labeled \mathcal{R}_{sc}° includes only isotropic interactions, while another, labeled $\mathcal{R}_{sc}^{\wedge}$, incorporates correlation-network interactions for

monomer–solvent and solvent–cosolvent pairs (Eq. (3)). The chain collapse observed for \mathcal{R}_{sc}° is consistent with a preferential mixing (PM) mechanism, with the most compact state being observed when the cosolvent to solvent ratio is balanced (Fig. 3b). Meanwhile, the collapse for \mathcal{R}_{sc}^\wedge aligns with a more nuanced geometric frustration (GF) mechanism (Fig. 3c). These results highlight how different cononsolvency mechanisms arise not only from distinct energetic regimes but also the specific nature of microscopic interactions.

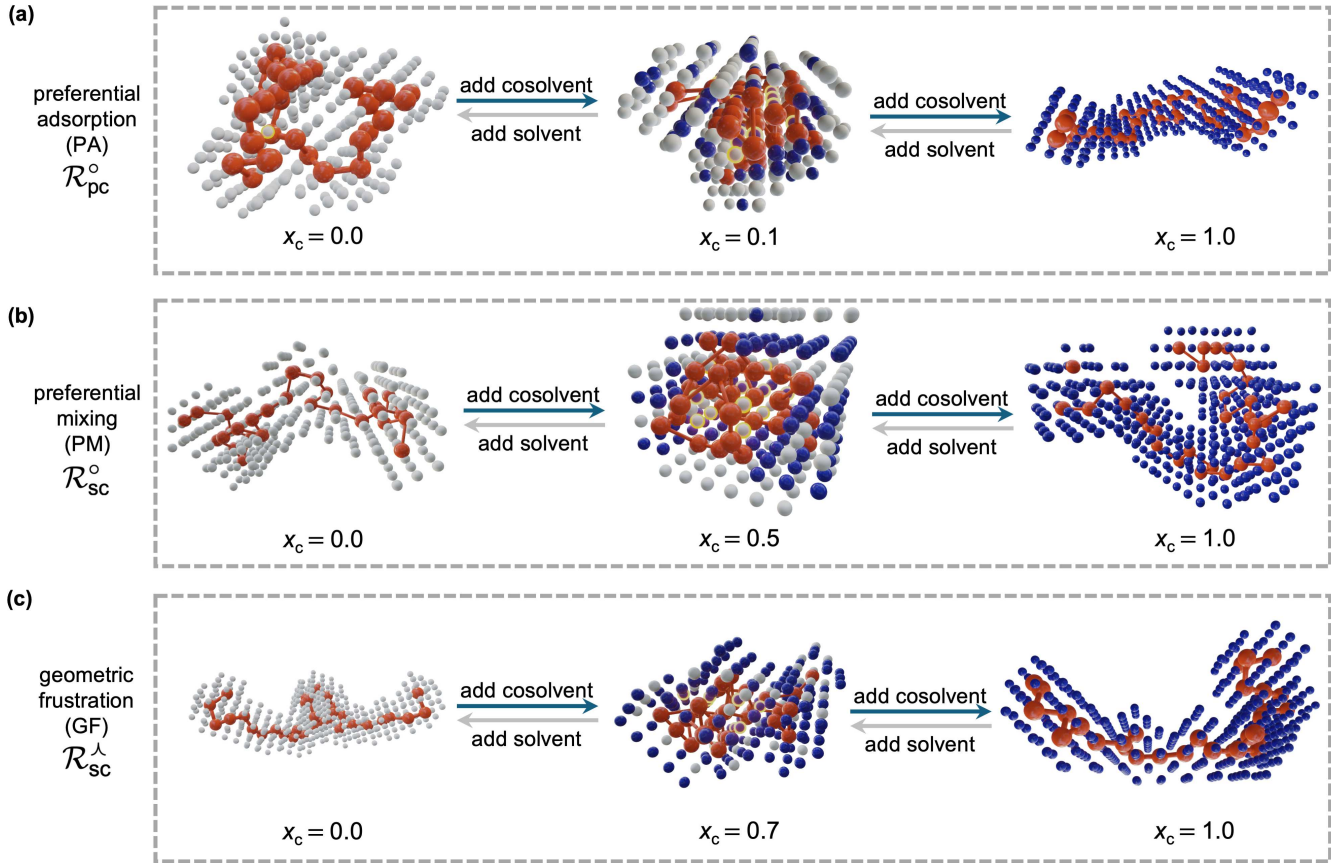


Figure 3: Single-chain conformations and solvation environments for distinct cononsolvency mechanisms. Molecular renderings from Monte Carlo simulations at specific mole fractions of cosolvent x_c for mechanisms labeled as (a) preferential adsorption (PA), (b) preferential mixing (PM), and (c) geometric frustration (GF). In all panels, only the polymer and particles within its first solvation shell are shown. The polymer is colored orange, the solvent as white, and the cosolvent as blue. Yellow outlines are used to highlight solvent and cosolvent particles that are within the first solvation shell of at least 8 monomers.

3.2.2 Chain collapse by preferential adsorption of cosolvent

In systems where polymer–cosolvent interactions are strongly favored (\mathcal{R}_{pc}°), the polymer is relatively collapsed in mixed solvents, with the greatest suppression of chain size occurring at low cosolvent mole fractions. This produces an asymmetric R_g profile as a function of composition (Fig. 4a). The chain is first swollen in pure solvent, collapses in the presence of small fractions of cosolvent, and gradually expands as additional cosolvent improves the overall solvent quality (Fig. 3a). Analysis of the solvation environment of the chain also reveals that the collapsed state is a relatively wet globule. This is demonstrated by the relative enrichment in cosolvent–monomer interactions (Fig. 4b) compared to the number of monomer–monomer interactions (Fig. 4d). Visually, cosolvent is embedded within the collapsed polymer chain so as to interact with multiple polymer segments (see highlighted particles in Fig. 3a). Trends for solvent–cosolvent interactions essentially follow ideal behavior (Fig. 4c), which is expected. Altogether, this suggests that the polymer chain attains a relatively compact state wherein cosolvent is intercalated between chain segments, limiting monomer–monomer interactions. These observations are broadly consistent with what has been described as the preferential adsorption (PA) mechanism.⁵¹

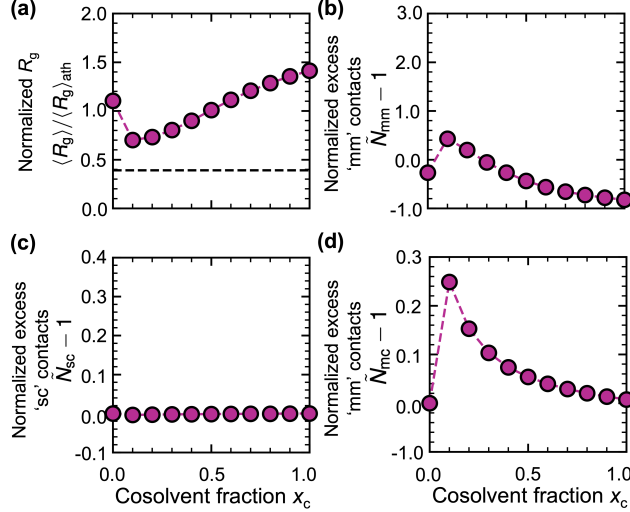


Figure 4: Analysis of system \mathcal{R}_{pc}° characterized by isotropic interactions and strong polymer-cosolvent affinity. The behavior as a function of cosolvent mole fraction for (a) normalized single-chain radius of gyration and normalized excess (b) monomer-monomer, (c) solvent-cosolvent, and (d) monomer-cosolvent interactions. In (a), the dashed horizontal line is a guide for the reference to a maximally compact polymer. Error bars correspond to the standard error of the mean and are generally smaller than the symbol size.

3.2.3 Chain collapse by preferential mixing of solvent and cosolvent

Chain collapse is also observed in systems where solvent-cosolvent interactions are strongly favorable (\mathcal{R}_{sc}°). In contrast to the behavior associated with the PA mechanism, the reduction in R_g is most pronounced when the solvent-to-cosolvent number ratio is closer to unity. This behavior coincides with nearly equimolar mixtures for which entropy of mixing is maximized, resulting in a more symmetric R_g profile as a function of cosolvent mole fraction (Fig. 5a). Notably, at $x_c \approx 0.5$, the chain adopts a size comparable to that observed for the PA mechanism ($x_c \approx 0.1$ in Fig. 4a). However, the globule here is more dry and lacks intercalated solvent (Fig. 3b); this is reflected by a marked increase in monomer-monomer interactions (Fig. 5b). Meanwhile, the number of solvent-cosolvent interactions is enhanced relative to an ideal mixture (Fig. 5c), and monomer-cosolvent interactions are somewhat suppressed (Fig. 5d). Together, these observations indicate that the polymer collapses into a conformation that largely excludes both solvent and cosolvent. This loss of conforma-

tional entropy is then offset by favorable solvent–cosolvent interactions, suggestive of the mechanism of preferential-mixing-induced (PM) cononsolvency.⁵¹

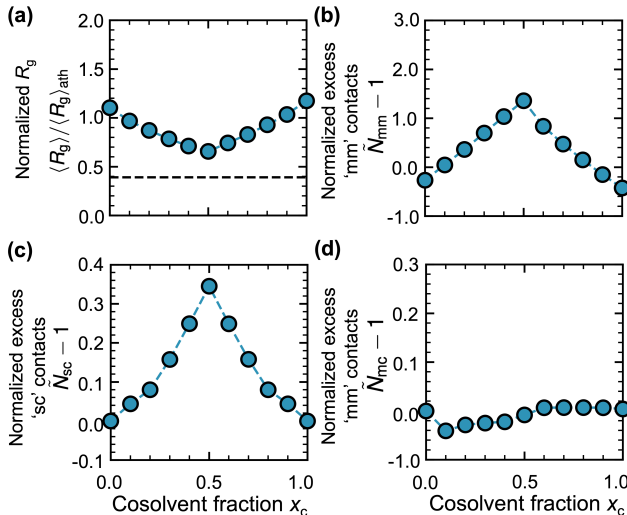


Figure 5: Analysis of system \mathcal{R}_{sc}^o characterized by isotropic interactions and strong polymer cosolvent affinity. The behavior as a function of cosolvent mole fraction for (a) normalized single-chain radius of gyration and normalized excess (b) monomer–monomer, (c) solvent–cosolvent, and (d) monomer–cosolvent interactions. In (a), the dashed horizontal line is a guide for the reference to a maximally compact polymer. Error bars correspond to the standard error of the mean and are generally smaller than the symbol size.

3.2.4 Chain collapse by geometric frustration of solvation

We now examine another system for which solvent–cosolvent interactions are strongly favorable according to \mathbf{X}^{FHP} . However, by contrast to the previous section that featured purely isotropic interactions, here we introduce a correlation-network alignment function ($\Lambda_{\text{corr}}, p_v = 1$) for both monomer–solvent and solvent–cosolvent interactions to consider implications of anisotropy. This is motivated by the observation that several systems that exhibit cononsolvency also display complex thermoresponsive behavior (e.g., lower-critical-solution temperatures and heating-induced coil–globule transitions) in pure solvents, and we have recently shown that anisotropic interactions are necessary to observe such behaviors within incompressible FHP models.⁶⁰

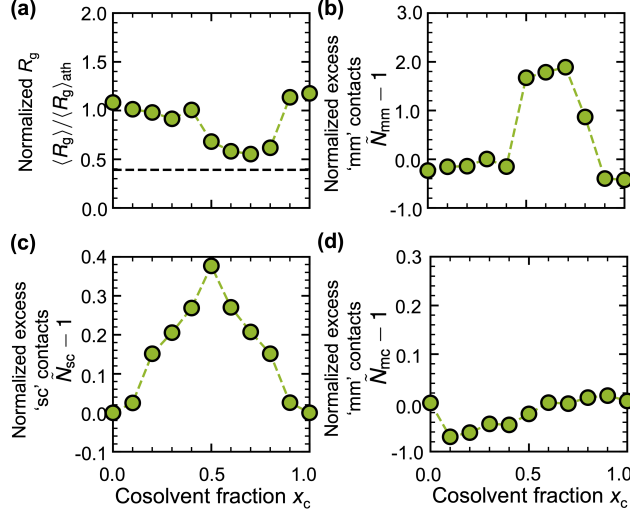


Figure 6: Analysis of system \mathcal{R}_{sc}^λ characterized by anisotropic interactions between polymer-solvent and solvent-cosolvent. The behavior as a function of cosolvent mole fraction for (a) normalized single-chain radius of gyration and normalized excess (b) monomer-monomer, (c) solvent-cosolvent, and (d) monomer-cosolvent interactions. In (a), the dashed horizontal line is a guide for the reference to a maximally compact polymer. Error bars correspond to the standard error of the mean and are generally smaller than the symbol size.

Compared to the behavior for the PM mechanism, the $\langle R_g \rangle / \langle R_g \rangle_{\text{ath}}$ profile for systems with anisotropic interactions is more asymmetric (Fig. 6a), with a minimum near $x_c \approx 0.7$. Furthermore, whereas the PM mechanism was characterized by a gradual collapse and then reexpansion as a function of cosolvent composition, the collapse from the coil state in this profile is more sudden, irrespective of whether approached from either the pure solvent or pure cosolvent side. Furthermore, the collapsed state is persistent over some composition range and also relatively dry based on the increase in excess monomer–monomer interactions (Fig. 6b). This collapse is also notable offest from the condition where solvent–cosolvent mixing is most strongly favorable, as evidenced by the behavior of the excess solvent-cosolvent interactions (Fig. 6c), which is similar to the PM mechanism. Furthermore, the behavior of excess monomer-cosolvent interactions (Fig. 6d) and the more persistent collapsed state differs from observations for PA. Thus, this mechanism is characterized by the chain remaining solvated even at optimal solvent–cosolvent mixing, then transitioning into a stable collapsed

state over a finite composition range with little change in size.

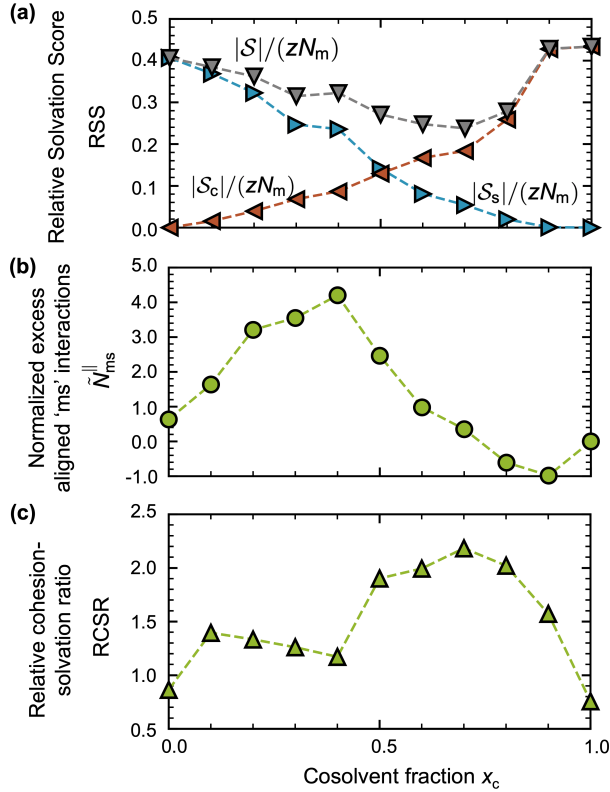


Figure 7: Solvation shell and interaction analysis for the system \mathcal{R}_{sc}^λ . (a) Relative solvation score $|\mathcal{S}|/(zN_m)$ (gray, inverted triangles), together with the individual solvent contribution $|\mathcal{S}_s|/(zN_m)$ (blue, right-pointing triangles) and cosolvent contribution $|\mathcal{S}_c|/(zN_m)$ (brown left-pointing triangles). (b) Normalized aligned monomer–solvent contact count $\tilde{N}_{ms}^{\parallel}$. (c) Relative cohesion–solvation ratio (RCSR). In all panels the horizontal axis denotes the cosolvent mole fraction x_c . Error bars (standard error of the mean over 30 independent simulations) are smaller than the plot symbols.

To elucidate the origin of the observed coil–globule transition behavior, we analyze the composition and structure of the polymer solvation shell. To assess composition, we decompose a relative solvation score (RSS) to quantify how well each monomer is solvated under given conditions (Fig. 7a), relative to full solvent exposure. While polymer exposure to cosolvent increases with x_c (brown, left-pointing triangles), it does not offset the loss of solvent exposure (blue, right-pointing triangles). The deficit in total solvation (gray, inverted triangles) is most pronounced for $x_c \in [0.5, 0.8]$, which coincides with the range of stable polymer collapse (Fig. 6a). In that same region, the total RSS reaches its minimum before recovering

at $x_c = 0.9$ to a value that exceeds its low- x_c baseline. This indicates that competition between solvent–cosolvent and solvent–monomer contacts underlies the initial downturn in RSS.

To better understand what may underlie this competition, we examine changes to the structure of the solvation shell. In particular, the number of aligned monomer–solvent interactions, $\tilde{N}_{\text{ms}}^{\parallel}$, increases relative to expectations from ideal mixing over the range of $x_c \leq 0.4$ (Fig. 7b). Because such interactions are favorable compared to misaligned monomer–solvent and monomer–cosolvent interactions (Table 1), this enhancement partially compensates for reduced solvent exposure. This suggests that despite loss of solvent, the solvent particles maintain and enhance cooperative alignment with the polymer on initial addition of cosolvent. Beyond $x_c = 0.4$, monomer–solvent alignment declines, as the overall abundance of cosolvent and the propensity for solvent–cosolvent mixing disrupts the cooperative organization observed at lower x_c . This tension is ultimately expressed through a relative cohesion-solvation ratio (RCSR) that examines a balance of drivers towards collapse (monomer–monomer and solvent–cosolvent interactions) and solvation (monomer–solvent and monomer–cosolvent interactions). The RCSR decreases slightly as monomer–solvent alignment increases up to $x_c = 0.4$, then rises when alignment is lost and continues increasing to $x_c = 0.8$ (Fig. 7c).

Collectively, we interpret these results as follows. First, the delayed collapse occurs because strong monomer–solvent alignment initially stabilizes the coil state; loss of alignment due to increasing prevalence of cosolvent induces collapse. Because monomer–monomer interactions are nominally constant in the collapsed state and the excess number of solvent–cosolvent interactions are decreasing (Fig. 6), the implication is that solvent–cosolvent alignment sustains the globular state. Finally, as solvent becomes increasingly scarce, this condition can no longer prevail, and monomer–cosolvent interactions again promote solvation, leading to the fall in RCSR. Therefore, given the competition of monomer–solvent and solvent–cosolvent

interactions that dictate the coil-globule and globule-coil transitions, we associate this regime with the notion of geometric frustration (GF).^{47,48}

4 Conclusion

We investigated the behavior of a range of Flory–Huggins–Potts models to better understand the signatures and origins of cononsolvency at both macroscopic and microscopic levels. The use of Flory-Huggins-Potts models was of interest to study the influence of interaction anisotropy on such behavior. Using mean-field analysis, we determined that macroscopic phase separation arises whenever polymer–solvent, polymer–cosolvent, or solvent–cosolvent interactions are relatively imbalanced relative to other energetic terms. We then connected these macroscopic signatures to single-chain behavior, showing how cosolvent-induced coil–globule transitions are observed for specific systems drawn from the aforementioned interaction regimes.

By analyzing facets of chain conformation, system energetics, and solvation shell composition, we associated particular parameter sets with certain mechanisms of cononsolvency, at the single-chain level. Preferential adsorption and preferential mixing both emerge from systems with purely isotropic pairwise interactions, whereas a mechanism resembling geometric frustration emerged when including anisotropic interactions. While preferential adsorption arises when monomer–solvent or monomer–cosolvent interactions dominate, both preferential mixing and geometric frustration occur for solvent–cosolvent–dominant regimes. This makes the distinction between the latter two mechanisms possibly challenging. The link between microscopic and macroscopic behavior, as well as the distinctions among mechanisms, was established within a single theoretical framework that relies on a well-defined set of interactions. Collectively, these results provide a unified perspective on cononsolvency of polymer solutions at a phenomenological level.

The insights and theoretical framework provided here may help distinguish cononsolvency

mechanisms and guide analysis of chemically realistic systems in both simulation and experiment. Our results generally support the idea that dominant interaction regimes can be inferred from binodal shapes and tie-line orientations, as previously suggested.⁵⁰ However, these observations cannot definitively separate preferential mixing from geometric frustration, since both derive from the same mean-field interaction parameters. Because geometric frustration requires interaction anisotropy, we expect their ternary phase diagrams to begin to differ when temperature is varied.

At the microscopic level, preferential adsorption produces an asymmetric R_g profile and a relatively “wet” globule with intercalated solvent. In contrast, both preferential mixing and geometric frustration yield “dry” globules. Between these two, geometric frustration typically leads to a more abrupt and more asymmetric collapse in R_g versus composition. This asymmetric collapse could resemble preferential adsorption, except that preferential adsorption appears characterized by a more gradual re-expansion as the cosolvent composition continues to change. We suggest that multi-modal characterization, as a function of temperature and system composition, should provide sufficient information to discriminate among mechanisms. Techniques such as scattering to probe chain structure, NMR spectroscopy to assess solvent distribution and dynamics, and cloud-point/turbidity measurements may be useful in this regard.

Acknowledgments

S.D. and M.A.W. acknowledge support from the National Science Foundation under Grant No. 2237470. Calculations were performed using resources from Princeton Research Computing at Princeton University, which is a consortium led by the Princeton Institute for Computational Science and Engineering (PICSciE) and Office of Information Technology’s Research Computing.

Data availability

The data and code associated with this study are publicly accessible at <https://github.com/webbtheosim/MCLATTE-public>.

Supporting Information

Monte Carlo simulation details. Convergence checks on Monte Carlo simulations.

References

1. Heskins, M.; Guillet, J. E. Solution Properties of Poly(N-isopropylacrylamide). *Journal of Macromolecular Science: Part A - Chemistry* **1968**, *2*, 1441–1455.
2. Bharadwaj, S.; Niebuur, B.-J.; Nothdurft, K.; Richtering, W.; van der Vegt, N. F. A.; Papadakis, C. M. Cononsolvency of thermoresponsive polymers: where we are now and where we are going. *Soft Matter* **2022**, *18*, 2884–2909.
3. Takahashi, N.; Kanaya, T.; Nishida, K.; Kaji, K. Effects of cononsolvency on gelation of poly(vinyl alcohol) in mixed solvents of dimethyl sulfoxide and water. *Polymer* **2003**, *44*, 4075–4078.
4. Jia, D.; Muthukumar, M.; Cheng, H.; Han, C. C.; Hammouda, B. Concentration Fluctuations near Lower Critical Solution Temperature in Ternary Aqueous Solutions. *Macromolecules* **2017**, *50*, 7291–7298.
5. Fernández-Piérola, I.; Horta, A. Co-nonsolvency of PMMA. *Polymer Bulletin* **1980**, *3*, 273–278.
6. Wang, F.; Shi, Y.; Luo, S.; Chen, Y.; Zhao, J. Conformational Transition of Poly(N-isopropylacrylamide) Single Chains in Its Cononsolvency Process: A Study by Fluores-

- cence Correlation Spectroscopy and Scaling Analysis. *Macromolecules* **2012**, *45*, 9196–9204.
7. Zhang, G.; Wu, C. The Water/Methanol Complexation Induced Reentrant Coil-to-Globule-to-Coil Transition of Individual Homopolymer Chains in Extremely Dilute Solution. *Journal of the American Chemical Society* **2001**, *123*, 1376–1380.
 8. Zhao, Y.; Kremer, K. The Effects of Proline Isomerization on the Solvation Behavior of Elastin-Like Polypeptides in Water–Ethanol Mixtures. *Macromolecular Rapid Communications* **2022**, *43*, 2100907.
 9. Zhao, Y.; Kremer, K. Proline Isomerization Regulates the Phase Behavior of Elastin-Like Polypeptides in Water. *The Journal of Physical Chemistry B* **2021**, *125*, 9751–9756.
 10. Hao, J.; Cheng, H.; Butler, P.; Zhang, L.; Han, C. C. Origin of cononsolvency, based on the structure of tetrahydrofuran-water mixture. *The Journal of Chemical Physics* **2010**, *132*, 154902.
 11. Sun, S.; Wu, P. Role of Water/Methanol Clustering Dynamics on Thermosensitivity of Poly(N-isopropylacrylamide) from Spectral and Calorimetric Insights. *Macromolecules* **2010**, *43*, 9501–9510.
 12. Hore, M. J. A.; Hammouda, B.; Li, Y.; Cheng, H. Co-Nonsolvency of Poly(n-isopropylacrylamide) in Deuterated Water/Ethanol Mixtures. *Macromolecules* **2013**, *46*, 7894–7901.
 13. Jia, D.; Zuo, T.; Rogers, S.; Cheng, H.; Hammouda, B.; Han, C. C. Re-entrance of Poly(N,N-diethylacrylamide) in D₂O/d-Ethanol Mixture at 27 °C. *Macromolecules* **2016**, *49*, 5152–5159.
 14. Budkov, Y. A.; Kiselev, M. G. Flory-type theories of polymer chains under different external stimuli. *Journal of Physics: Condensed Matter* **2017**, *30*, 043001.

15. Pooch, F.; Teltevskij, V.; Karjalainen, E.; Tenhu, H.; Winnik, F. M. Poly(2-propyl-2-oxazoline)s in Aqueous Methanol: To Dissolve or not to Dissolve. *Macromolecules* **2019**, *52*, 6361–6368.
16. Zuo, T.; Ma, C.; Jiao, G.; Han, Z.; Xiao, S.; Liang, H.; Hong, L.; Bowron, D.; Soper, A.; Han, C. C.; Cheng, H. Water/Cosolvent Attraction Induced Phase Separation: A Molecular Picture of Cononsolvency. *Macromolecules* **2019**, *52*, 457–464.
17. Yong, H.; Bittrich, E.; Uhlmann, P.; Fery, A.; Sommer, J.-U. Co-Nonsolvency Transition of Poly(N-isopropylacrylamide) Brushes in a Series of Binary Mixtures. *Macromolecules* **2019**, *52*, 6285–6293.
18. Zhang, Y.; Carvalho, W. S.; Fang, C.; Serpe, M. J. Volatile organic compound vapor detection with responsive microgel-based etalons. *Sensors and Actuators B: Chemical* **2019**, *290*, 520–526.
19. Nian, S.; Pu, L. Racemic Fluorescence Probe for Enantiomeric Excess Determination: Application of Cononsolvency of a Polymer in Sensing. *The Journal of Organic Chemistry* **2018**, *84*, 909–913.
20. Kleinschmidt, D.; Nothdurft, K.; Anakhov, M. V.; Meyer, A. A.; Mork, M.; Gumerov, R. A.; Potemkin, I. I.; Richtering, W.; Pich, A. Microgel organocatalysts: modulation of reaction rates at liquid–liquid interfaces. *Materials Advances* **2020**, *1*, 2983–2993.
21. Yu, Y.; Cirelli, M.; Kieviet, B. D.; Kooij, E. S.; Vancso, G. J.; de Beer, S. Tunable friction by employment of co-non-solvency of PNIPAM brushes. *Polymer* **2016**, *102*, 372–378.
22. Chen, Q.; Kooij, E. S.; Sui, X.; Padberg, C. J.; Hempenius, M. A.; Schön, P. M.; Vancso, G. J. Collapse from the top: brushes of poly(N-isopropylacrylamide) in cononsolvent mixtures. *Soft Matter* **2014**, *10*, 3134.

23. Wang, X.; Huang, H.; Liu, H.; Rehfeldt, F.; Wang, X.; Zhang, K. Multi-Responsive Bilayer Hydrogel Actuators with Programmable and Precisely Tunable Motions. *Macromolecular Chemistry and Physics* **2019**, *220*.
24. Yong, H.; Molcrette, B.; Sperling, M.; Montel, F.; Sommer, J.-U. Regulating the Translocation of DNA through Poly(N-isopropylacrylamide)-Decorated Switchable Nanopores by Cononsolvency Effect. *Macromolecules* **2021**, *54*, 4432–4442.
25. Mills, C. E.; Ding, E.; Olsen, B. Protein Purification by Ethanol-Induced Phase Transitions of the Elastin-like Polypeptide (ELP). *Industrial & Engineering Chemistry Research* **2019**, *58*, 11698–11709.
26. Valente, J. J.; Verma, K. S.; Manning, M. C.; William Wilson, W.; Henry, C. S. Second Virial Coefficient Studies of Cosolvent-Induced Protein Self-Interaction. *Biophysical Journal* **2005**, *89*, 4211–4218.
27. Xiao, T.; Gardner, K. H.; Sprang, S. R. Cosolvent-induced transformation of a death domain tertiary structure. *Proceedings of the National Academy of Sciences* **2002**, *99*, 11151–11156.
28. Reddy, G.; Muttathukattil, A. N.; Mondal, B. Cosolvent effects on the growth of amyloid fibrils. *Current Opinion in Structural Biology* **2020**, *60*, 101–109.
29. Canchi, D. R.; García, A. E. Cosolvent Effects on Protein Stability. *Annual Review of Physical Chemistry* **2013**, *64*, 273–293.
30. Gazi, R.; Maity, S.; Jana, M. Conformational Features and Hydration Dynamics of Proteins in Cosolvents: A Perspective from Computational Approaches. *ACS Omega* **2023**, *8*, 2832–2843.
31. Stuart, M. A. C.; Huck, W. T. S.; Genzer, J.; Müller, M.; Ober, C.; Stamm, M.; Sukhorukov, G. B.; Szleifer, I.; Tsukruk, V. V.; Urban, M.; Winnik, F.; Zauscher, S.; Luzi-

- nov, I.; Minko, S. Emerging applications of stimuli-responsive polymer materials. *Nature Materials* **2010**, *9*, 101–113.
32. Nettles, D. L.; Chilkoti, A.; Setton, L. A. Applications of elastin-like polypeptides in tissue engineering. *Advanced Drug Delivery Reviews* **2010**, *62*, 1479–1485.
33. Rodríguez-Cabello, J. C.; Arias, F. J.; Rodrigo, M. A.; Girotti, A. Elastin-like polypeptides in drug delivery. *Advanced Drug Delivery Reviews* **2016**, *97*, 85–100.
34. Mukherji, D.; Marques, C. M.; Stuehn, T.; Kremer, K. Co-non-solvency: Mean-field polymer theory does not describe polymer collapse transition in a mixture of two competing good solvents. *The Journal of Chemical Physics* **2015**, *142*, 114903.
35. Tanaka, F. The polymer-induced coil–globule transition. *The Journal of Chemical Physics* **1985**, *82*, 2466–2471.
36. Tanaka, T.; Nishio, I.; Sun, S.-T.; Ueno-Nishio, S. Collapse of Gels in an Electric Field. *Science* **1982**, *218*, 467–469.
37. Tanaka, F.; Koga, T.; Winnik, F. M. Temperature-Responsive Polymers in Mixed Solvents: Competitive Hydrogen Bonds Cause Cononsolvency. *Physical Review Letters* **2008**, *101*, 028302.
38. Tanaka, F.; Koga, T.; Kojima, H.; Xue, N.; Winnik, F. M. Preferential Adsorption and Co-nonsolvency of Thermoresponsive Polymers in Mixed Solvents of Water/Methanol. *Macromolecules* **2011**, *44*, 2978–2989.
39. Dalgicdir, C.; van der Vegt, N. F. A. Improved Temperature Behavior of PNIPAM in Water with a Modified OPLS Model. *The Journal of Physical Chemistry B* **2019**, *123*, 3875–3883.

40. Pérez-Ramírez, H. A.; Haro-Pérez, C.; Vázquez-Contreras, E.; Klapp, J.; Bautista-Carbajal, G.; Odriozola, G. P-NIPAM in water–acetone mixtures: experiments and simulations. *Physical Chemistry Chemical Physics* **2019**, *21*, 5106–5116.
41. Budkov, Y. A.; Kolesnikov, A. L. Models of the Conformational Behavior of Polymers in Mixed Solvents. *Polymer Science, Series C* **2018**, *60*, 148–159.
42. Budkov, Y. A.; Kolesnikov, A. L. Statistical description of co-nonsolvency suppression at high pressures. *Soft Matter* **2017**, *13*, 8362–8367.
43. Bharadwaj, S.; van der Vegt, N. F. A. Does Preferential Adsorption Drive Cononsolvency? *Macromolecules* **2019**, *52*, 4131–4138.
44. Bharadwaj, S.; Nayar, D.; Dalgicdir, C.; van der Vegt, N. F. A. A cosolvent surfactant mechanism affects polymer collapse in miscible good solvents. *Communications Chemistry* **2020**, *3*.
45. Dudowicz, J.; Freed, K. F.; Douglas, J. F. Theory of competitive solvation of polymers by two solvents and entropy-enthalpy compensation in the solvation free energy upon dilution with the second solvent. *The Journal of Chemical Physics* **2015**, *142*.
46. Wang, J.; Wang, N.; Liu, B.; Bai, J.; Gong, P.; Ru, G.; Feng, J. Preferential adsorption of the additive is not a prerequisite for cononsolvency in water-rich mixtures. *Physical Chemistry Chemical Physics* **2017**, *19*, 30097–30106.
47. Pica, A.; Graziano, G. An alternative explanation of the cononsolvency of poly(N-isopropylacrylamide) in water–methanol solutions. *Physical Chemistry Chemical Physics* **2016**, *18*, 25601–25608.
48. Dalgicdir, C.; Rodríguez-Ropero, F.; van der Vegt, N. F. A. Computational Calorimetry of PNIPAM Cononsolvency in Water/Methanol Mixtures. *The Journal of Physical Chemistry B* **2017**, *121*, 7741–7748.

49. Dudowicz, J.; Freed, K. F.; Douglas, J. F. Communication: Cosolvency and cononsolvency explained in terms of a Flory-Huggins type theory. *The Journal of Chemical Physics* **2015**, *143*, 131101.
50. Zhang, P. Phase Separation of Homopolymers in Binary Mixed Solvents-The Cononsolvency Effect. *Macromolecules* **2024**, *57*, 4298–4311.
51. Zhang, X.; Zong, J.; Meng, D. A unified understanding of the cononsolvency of polymers in binary solvent mixtures. *Soft Matter* **2020**, *16*, 7789–7796.
52. Bharadwaj, S.; Nayar, D.; Dalgicdir, C.; van der Vegt, N. F. A. An interplay of excluded-volume and polymer-(co)solvent attractive interactions regulates polymer collapse in mixed solvents. *The Journal of Chemical Physics* **2021**, *154*.
53. Mukherji, D.; Marques, C. M.; Kremer, K. Polymer collapse in miscible good solvents is a generic phenomenon driven by preferential adsorption. *Nature Communications* **2014**, *5*.
54. Sommer, J.-U. Adsorption–Attraction Model for Co-Nonsolvency in Polymer Brushes. *Macromolecules* **2017**, *50*, 2219–2228.
55. Sommer, J.-U. Gluonic and Regulatory Solvents: A Paradigm for Tunable Phase Segregation in Polymers. *Macromolecules* **2018**, *51*, 3066–3074.
56. Mukherji, D.; Wagner, M.; Watson, M. D.; Winzen, S.; de Oliveira, T. E.; Marques, C. M.; Kremer, K. Relating side chain organization of PNIPAm with its conformation in aqueous methanol. *Soft Matter* **2016**, *12*, 7995–8003.
57. Pica, A.; Graziano, G. Comment on “Relating side chain organization of PNIPAm with its conformation in aqueous methanol” by D. Mukherji, M. Wagner, M. D. Watson, S. Winzen, T. E. de Oliveira, C. M. Marques and K. Kremer, *Soft Matter*, 2016, *12*, 7995. *Soft Matter* **2017**, *13*, 7698–7700.

58. van der Vegt, N. F. A.; Rodríguez-Ropero, F. Comment on “Relating side chain organization of PNIPAm with its conformation in aqueous methanol” by D. Mukherji, M. Wagner, M. D. Watson, S. Winzen, T. E. de Oliveira, C. M. Marques and K. Kremer, *Soft Matter*, 2016, 12, 7995. *Soft Matter* **2017**, 13, 2289–2291.
59. Mukherji, D.; Wagner, M.; Watson, M. D.; Winzen, S.; de Oliveira, T. E.; Marques, C. M.; Kremer, K. Reply to the ‘Comment on “Relating side chain organization of PNIPAm with its conformation in aqueous methanol”’ by A. Pica and G. Graziano, *Soft Matter*, 2017, 13, DOI: 10.1039/C7SM01065F. *Soft Matter* **2017**, 13, 7701–7703.
60. Dhamankar, S.; Webb, M. A. Asymmetry in Polymer–Solvent Interactions Yields Complex Thermoresponsive Behavior. *ACS Macro Letters* **2024**, 13, 818–825.
61. van der Schoot, P. *Molecular Theory of Nematic (and Other) Liquid Crystals*; Springer International Publishing, 2022; pp 57–69.
62. Scott, R. L. The Thermodynamics of High Polymer Solutions. IV. Phase Equilibria in the Ternary System: Polymer—Liquid 1—Liquid 2. *The Journal of Chemical Physics* **1949**, 17, 268–279.
63. Tompa, H. The Critical Points of Ternary Systems with a Polymer Component. *The Journal of Chemical Physics* **1949**, 17, 1006–1006.
64. Dhamankar, S.; Jiang, S.; Webb, M. A. Accelerating multicomponent phase-coexistence calculations with physics-informed neural networks. *Molecular Systems Design & Engineering* **2025**, 10, 89–101.
65. Jin, T.; Coley, C. W.; Alexander-Katz, A. Designing single-polymer-chain nanoparticles to mimic biomolecular hydration frustration. *Nature Chemistry* **2025**,

Supporting Information for

Towards a Unified Understanding of Polymer Cononsolvency: Insights from the Flory-Huggins-Potts framework

Satyen Dhamankar, Michael A. Webb
Corresponding email: mawebb@princeton.edu

Contents

SI. Monte Carlo simulation details.

Table. S1. Summary of Monte Carlo moves employed in the simulations. Moves either modify the position and/or orientation of selected particles on the lattice.

Fig. S1. Equilibration behavior for the three mechanisms of cononsolvency: preferential adsorption (PA), preferential mixing (PM), and geometric frustration (GF). Panels (a–c) show the autocorrelation function of the radius of gyration over the final 5×10^7 moves at (a) $x_c = 0.0, 0.1$, and 1.0 for PA; (b) $x_c = 0.005$, and 1.0 for PM; and (c) $x_c = 0.0, 0.7$, and 1.0 for GF. Panels (d–f) show block-averaged radius of gyration (8 blocks) for the same conditions. Results are based on thirty independent simulations. Error bars (standard error) are smaller than the symbols.

S1 Monte Carlo simulation details and convergence

Simulations are conducted on a $34 \times 34 \times 34$ simple cubic lattice with periodic boundary conditions. The lattice is populated by solvent particles and a single polymer chain of length $N_m = 32$. We employ a coordination number $z = 26$, incorporating interactions with nearest, next-nearest, and next-next-nearest neighbors. Particle orientations are restricted to directions pointing toward these 26 neighboring sites. Monte Carlo (MC) moves for solvent particles include exchanges of orientation between neighboring solvent sites and collective orientation perturbations. For the polymer chain, MC updates involve end-rotation, reptation, orientation changes, and chain regrowth accompanied by orientation perturbations. The full set of MC moves is summarized in Table S1, with each move type selected at equal probability. Chain regrowth moves are performed using a Rosenbluth sampling method to improve sampling efficiency. Each simulation runs for 10^8 MC moves, with the second half used for data analysis. Reported averages are based on 30 independent simulations, and all error bars denote the standard error of the mean.

Table S1: Summary of Monte Carlo moves employed in the simulations. Moves either modify the position and/or orientation of selected particles on the lattice.

	Move type	Move description
1	End rotation	The polymer end segments, m_1 and m_M , are randomly selected and attempt to exchange with a neighboring solvent site adjacent to m_2 or m_{M-1} , respectively.
2	Reptation (‘slithering snake’)	An end monomer (m_1 or m_M) is chosen uniformly, and the polymer is shifted in a direction. The move is accepted if the chain advances into its other end’s former location or displaces a solvent particle.
3	Chain regrowth with orientation adjustment	A monomer index i between 2 and $M - 1$ is picked uniformly. If $ M - i < i - 1 $, monomers $m_{i+1}, m_{i+2}, \dots, m_M$ are repositioned and reoriented; if $ M - i > i - 1 $, then monomers m_1, m_2, \dots, m_{i-1} are modified instead. If $ M - i = i - 1 $, one of the two possible segments is randomly selected.
4	Chain regrowth without orientation adjustment	A monomer index i between 2 and $M - 1$ is selected uniformly. If $ M - i < i - 1 $, monomers $m_{i+1}, m_{i+2}, \dots, m_M$ are repositioned only; if $ M - i > i - 1 $, monomers m_1, m_2, \dots, m_{i-1} are repositioned only; if $ M - i = i - 1 $, either set is chosen at random.
5	Polymer orientation perturbation	A random subset of polymer monomers has its orientations randomly perturbed.
6	Solvent orientation perturbation	Among the $(L/2)^3$ solvent particles, n are randomly selected and their orientations are perturbed.
7	Solvent exchange	Two solvent particles are chosen randomly and their positions are swapped.
8	Solvent exchange with orientation perturbation	Two solvent particles are randomly picked; their positions are exchanged and their orientations are randomly perturbed.
9	Solvation shell perturbation	Solvent particles directly contacting the polymer have their orientations perturbed.
10	Solvation shell exchange	A solvent particle near the polymer and another particle elsewhere in the system are selected and their positions are swapped.
11	Solvation shell exchange with orientation perturbation	A solvent particle near the polymer and a randomly chosen solvent particle elsewhere swap locations and both have their orientations randomly perturbed.

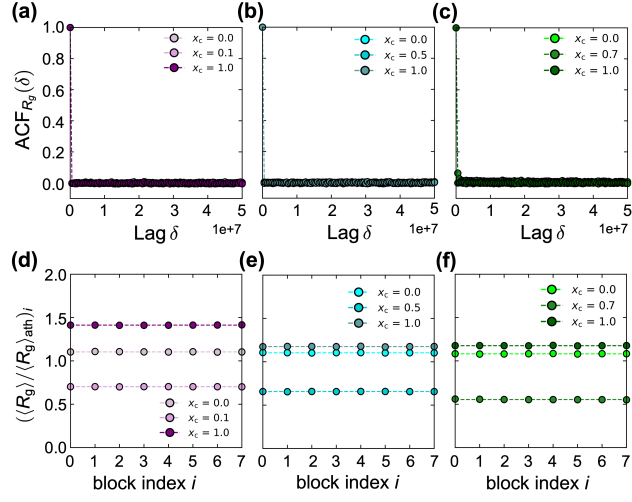


Figure S1: Equilibration checks for the three mechanisms of cononsolvency: preferential adsorption (PA), preferential mixing (PM), and geometric frustration (GF). Panels (a–c) show the autocorrelation function of the radius of gyration over the final 5×10^7 moves at (a) $x_c = 0.0, 0.1$, and 1.0 for PA; (b) $x_c = 0.0, 0.5$, and 1.0 for PM; and (c) $x_c = 0.0, 0.7$, and 1.0 for GF. Panels (d–f) show block-averaged normalized radius of gyration $\langle R_g \rangle / \langle R_g \rangle_{\text{ath}}$ (8 blocks) for the same conditions. Statistics are computed from thirty independent simulations. Error bars (standard error) are smaller than the symbols.